Analytical and Bioanalytical Chemistry (2024) 416:559–568
https://doi.org/10.1007/s00216-023-05063-1

RESEARCH PAPER

Potential of measured relative shifts in collision cross section values for biotransformation studies

Christian Lanshoeft[1] · Raphael Schütz[2] · Frédéric Lozac'h[1] · Götz Schlotterbeck[2,3] · Markus Walles[1]

Received: 25 September 2023 / Revised: 17 November 2023 / Accepted: 20 November 2023 / Published online: 2 December 2023

Abstract

Ion mobility spectrometry–mass spectrometry (IMS-MS) separates gas phase ions due to differences in drift time from which reproducible and analyte-specific collision cross section (CCS) values can be derived. Internally conducted in vitro and in vivo metabolism (biotransformation) studies indicated repetitive shifts in measured CCS values (CCS_{meas}) between parent drugs and their metabolites. Hence, the purpose of the present article was (i) to investigate if such relative shifts in CCS_{meas} were biotransformation-specific and (ii) to highlight their potential benefits for biotransformation studies. First, mean CCS_{meas} values of 165 compounds were determined (up to $n=3$) using a travelling wave IMS-MS device with nitrogen as drift gas ($^{TW}CCS_{N2,\ meas}$). Further comparison with their predicted values ($^{TW}CCS_{N2,\ pred}$, Waters CCSonDemand) resulted in a mean absolute error of 5.1%. Second, a reduced data set ($n=139$) was utilized to create compound pairs ($n=86$) covering eight common types of phase I and II biotransformations. Constant, discriminative, and almost non-overlapping relative shifts in mean $^{TW}CCS_{N2,\ meas}$ were obtained for demethylation (-6.5 ± 2.1 Å^2), oxygenation (hydroxylation $+3.8 \pm 1.4$ Å^2, N-oxidation $+3.4 \pm 3.3$ Å^2), acetylation ($+13.5 \pm 1.9$ Å^2), sulfation ($+17.9 \pm 4.4$ Å^2), glucuronidation (N-linked: $+41.7 \pm 7.5$ Å^2, O-linked: $+38.1 \pm 8.9$ Å^2), and glutathione conjugation ($+49.2 \pm 13.2$ Å^2). Consequently, we propose to consider such relative shifts in $^{TW}CCS_{N2,\ meas}$ (rather than absolute values) as well for metabolite assignment/confirmation complementing the conventional approach to associate changes in mass-to-charge (*m/z*) values between a parent drug and its metabolite(s). Moreover, the comparison of relative shifts in $^{TW}CCS_{N2,\ meas}$ significantly simplifies the mapping of metabolites into metabolic pathways as demonstrated.

Keywords Ion mobility spectrometry mass spectrometry · Collision cross section · Biotransformation assignment · Metabolite mapping · CCSonDemand

Introduction

Metabolism (biotransformation) refers to the biochemical conversion of endogenous and exogenous compounds from one form to another by specific enzymes aiming to increase their excretion from the body. Biotransformation studies are requested by the US Food and Drug Administration [1, 2], European Medicines Agency [3], or International Conference on Harmonization [4] to bring new drug candidates safely into patients. At discovery stage, metabolic liabilities within a drug candidate need to be investigated to optimize metabolic turnover. Objectives of in vitro and in vivo–conducted biotransformation studies at development stage cover (i) the identification of circulating metabolites in human and selected animal toxicity species, (ii) testing of their pharmacological activity, (iii) assessment of the presence of reactive or toxic metabolites, and (iv) mapping of metabolites into

✉ Christian Lanshoeft
christian.lanshoeft@novartis.com

[1] Biomedical Research, PK Sciences, Novartis Pharma AG, Fabrikstrasse 14 (Novartis Campus), 4056 Basel, Switzerland

[2] School of Life Sciences FHNW, Institute for Chemistry and Bioanalytics, University of Applied Sciences and Arts Northwestern Switzerland, Hofackerstrasse 30, 4132 Muttenz, Switzerland

[3] Department of Forensic Chemistry and Toxicology, Institute of Forensic Medicine, University of Basel, Pestalozzistrasse 22, 4056 Basel, Switzerland

metabolic pathways to elucidate elimination pathways [5–7]. Liquid chromatography–high-resolution mass spectrometry (LC-HRMS) represents the key analytical technology used for biotransformation studies [8–10]. Although LC-HRMS analysis offers a high degree of specificity for metabolite profiling and identification due to obtained retention times, mass-to-charge (*m/z*) ratios of precursor ions, their mass fragmentation, and exact mass measurements, several challenges remain. For instance, isobaric metabolites or structural isomers cannot readily be differentiated from each other solely based on the beforementioned physicochemical parameters due to (i) co-elution, (ii) similar MS, or (iii) MS2 spectral data. Moreover, low abundant in vivo metabolites can hardly be identified when highly abundant co-extracted interferences from matrix components, co-medications, or residual formulation entities are present causing ion suppression and increased detection limits. Lastly, the absence of radiotracers at early drug development stage further impedes a reliable and complete metabolite elucidation. Fortunately, the combination of ion mobility spectrometry (IMS) with mass spectrometry (MS) analysis (IMS-MS) introduces an additional analytical dimension to overcome some of the previously stated hurdles. IMS-MS enables the separation of ions in the gas phase due to differences in size, shape, and charge [11–13]. In the perspective of biotransformation studies, the application of LC-IMS-MS is beneficial in several ways: (i) Elucidation of in vivo metabolites can significantly be facilitated allowing the effective elimination of background ions from matrix components in the MS spectrum [14]. (ii) Positional and structural isomers can readily be separated using either linear [15, 16] or cyclic IMS-MS devices [17–19] exhibiting an increased IMS resolution [20]. (iii) Conformational changes of enzymes upon ligand binding can be assessed [21]. The determination of drift time-derived collision cross section (CCS) values, however, represents the major benefit for metabolism studies [12, 22]. Such robust and analyte-specific parameters allow simple identification and tracking of analytes across investigated matrices, different species, and studies [22]. Such alignment is particularly important when drug development spans over multiple years, compounds have been in-licensed, or biotransformation studies were not entirely conducted in-house (same analytical lab or instrument). Ross et al. [23] previously reported changes in measured CCS values (CCS_{meas}) between parent drugs and their in vitro metabolites which created the foundation of our presented work. Their earlier finding agreed with our internal data from various drug development projects. However, we further observed repetitive shifts in relative CCS_{meas} values between parent drugs (or precursors) with their corresponding in vitro or in vivo metabolites. In this publication, we present the outcome of our investigation demonstrating if such relative shifts in CCS_{meas} are biotransformation-specific and highlighting how such relative shifts in CCS_{meas} further benefit biotransformation studies.

Material and methods

Chemicals, reagents, and reference material

Formic acid (FA), MS grade water, and acetonitrile (ACN) were obtained from Fisher Chemicals (Loughborough, UK). Adenosine-3′-phosphate 5′ phosphate lithium salt (PAPS), dimethyl sulfoxide, leucine enkephalin acetate salt, reduced L-glutathione (GSH), poly-DL-alanine, and sodium formate were purchased from Sigma-Aldrich (Buchs, Switzerland). Potassium phosphate buffer (0.5 M, pH 7.4) was provided by Thermo Fisher Scientific (Allschwil, Switzerland). Pooled liver S9 fractions were purchased from either BioIVT (West Sussex, UK) or Corning (Woburn, MA, USA). Reference material of investigated compounds was obtained either commercially from various vendors (SI, Table S1) or was synthesized in-house. Due to proprietary reasons, drug names, development codes, batch numbers, or obtained *m/z* values of utilized internal reference material of active development compounds cannot be disclosed. Corresponding material was denoted as either *NVSx* (parent drugs) or *Mx* (metabolites). Moreover, molecular structures of selected internal compounds can only be shown partially.

Stock and working solutions

Reference material of commercial or internal compounds was first dissolved in dimethyl sulfoxide to obtain stock solutions at 1 mM. Individual stock solutions were further diluted in water/ACN (95/5, v/v) to obtain working solutions at 10 µM containing up to five different compounds. The selection of compounds, which were pooled into individual working solutions, was based on physicochemical properties (molecular weights, polarities, and ionization profiles). Moreover, neither isobaric metabolites (e.g., 10- and 2-hydroxy imipramine) nor metabolites which potentially get back-converted to the parent drug/precursor due to in-source fragmentation (e.g., sulfates and glucuronides) were merged together into the same working solution. No further sample preparation was required for CCS_{meas} determination.

In vitro incubations

Several parent drugs or precursors were incubated in pooled liver S9 fractions from *CD1 mice*, *Sprague–Dawley rats*, *cynomolgus monkeys*, or *humans* to generate specific metabolites for which no reference material was available (neither commercially nor internally). Deep-frozen pooled liver S9 fractions were first thawed at room temperature

and subsequently diluted in potassium phosphate buffer (100 mM, pH 7.4) containing either PAPS (4 mM) or GSH (5 mM) as a cofactor for sulfation or glutathione conjugation, respectively. Following preincubation on a Thermomixer C from Eppendorf (Hamburg, Germany) for 5 min at 37 °C while shaking at 600 rpm, incubations were initiated by adding either the parent drug or precursor (7-hydroxy coumarin, estradiol, raloxifene, and serotonin for sulfation while acalabrutinib, afatinib, branebrutinib, ibrutinib, rociletinib, and spebrutinib were used for GSH conjugation). The total incubation volume was 500 µL with a final protein and substrate concentration of 2 mg/mL and 10 µM, respectively. Following 2 h of incubation at 37 °C and 600 rpm (Thermomixer C), 100 µL of each incubate was drawn and the enzymatic activity was quenched with four volumes of ice-cold ACN. After centrifugation for 15 min at 4 °C and 18,000 g, 200 µL of each supernatant was transferred to a fresh 0.5 mL ProteinLobind tube (Eppendorf). The transferred supernatants were evaporated to dryness under a gentle stream of nitrogen (N_2) and reconstituted in 50 µL of water/ACN (95/5, v/v). Following brief agitation, each reconstituted supernatant was centrifuged again for 5 min at 4 °C and 18,000 g prior to metabolite profiling.

Preclinical plasma samples of NVS1

NVS1 was administrated once daily either orally (100 mg/kg for 112 days) or intravenously (5 mg/kg for 111 days) to twenty *Han Wistar* rats or six purebred *beagle* dogs, respectively. In both cases, mixed-gender animals were used. Rats were obtained from Charles River Laboratories (Raleigh, NC, USA) whereas dogs were received from Marshall BioResources (North Rose, NY, USA). Blood samples (300 µL for rat and 1 mL for dog) were drawn at 0.083 (dog only), 0.25 (rat only), 0.5 (dog only) 1, 3, 7, and 24 h post-dose into K2 EDTA-containing tubes. Plasma was harvested following centrifugation for 10 min at 2700 rpm and 4 °C. Regardless of the species, plasma pools (AUC0-24 h) were generated according to the pooling strategy proposed by Hamilton et al. [24]. Metabolite profiling of the protein-precipitated plasma pools was conducted by LC-HRMS analysis (SI, Table S2).

LC-IMS-MS analysis

CCS_{meas} determination and metabolite profiling were conducted with an Acquity I-Class UPLC system from Waters (Milford, MA, USA) coupled to a Waters Synapt G2-Si HD QTOF high-resolution mass spectrometer. Depending on the sample and experiment, 2–10 µL were injected onto a Waters Acquity UPLC HSS T3 column (2.1 × 150 mm, 1.8 µm) being maintained at 40 °C. The mobile phases consisted of 0.1% FA in water (A) and 0.1% FA in ACN (B). The elution gradient with a flow rate of 0.4 mL/min was set as follows: 0.0–1.0 min, 5% B; 7.8–8.5 min, 95% B; 8.6–10.0 min, 5% B. The minor part of the post-column split (1/5, v/v) was directed towards the mass spectrometer. The capillary voltage of the electrospray ionization (ESI) was either 3 kV (positive mode) or 2 kV (negative mode). The remaining IMS-MS parameters were set as follows: source temperature 120 °C, sampling cone voltage 10 V, cone gas flow rate 20 L/h (N_2), desolvation temperature 350 °C, desolvation gas flow rate 600 L/h (N_2), nebulizer gas pressure 6 bar, IMS gas flow rate 90 mL/min (N_2), IMS wave velocity and height at 500 m/s and 40 V, respectively. HDMS^e data were acquired in resolution mode using the continuum data format: full-scan (*m/z* 100–1200) with a scan time of 0.5 s either without (function 1) or with collision energy ramp from 10 to 50 eV in the transfer cell (function 2) of the TriWave device for precursor ion $^{TW}CCS_{N2}$ determination. For product ion $^{TW}CCS_{N2}$ determination, fixed collision energies (either 12 or 25 eV) were applied in the trap cell of the TriWave device on the low instead of high-energy MS trace while maintaining the same IMS-MS parameters as stated above. Mass and $^{TW}CCS_{N2}$ calibrations were fully automated (Waters IntelliStart application in the instrument console) and were conducted with 0.5 mM sodium formate in ACN/water (1/1, v/v) containing 0.1% FA and polyalanine solution at 20.0 µg/mL in ACN/water (1/1, v/v) containing acetaminophen at 5.00 µg/mL, respectively. Utilized reference $^{TW}CCS_{N2}$ values used to convert measured drift times of individual ions into corresponding $^{TW}CCS_{N2}$ values were previously published by Bush et al. [25]. Those values are further provided in the supplementary information (SI, Table S3). The entire LC-IMS-MS system was operated and controlled under Waters Masslynx (v4.2).

Prediction and determination of measured $^{TW}CCS_{N2}$ values

Mol files of the molecular structure from each investigated compound were generated with ChemDraw (v19.1) from PerkinElmer (Waltham, MA, USA) prior to their upload to CCSonDemand (Waters), a machine learning algorithm for $^{TW}CCS_{N2}$ value prediction ($^{TW}CCS_{N2,\ pred}$) [26, 27]. Measured $^{TW}CCS_{N2}$ values ($^{TW}CCS_{N2,\ meas}$) were determined with Waters Unifi (v1.9.4). For this, accurate mass screening on LC-IMS-MS data was performed with a mass accuracy of 20 ppm. The $[M+H]^+$ ion of leucine enkephalin at *m/z* 556.2766 and its drift time were further used for exact mass and CCS correction. Following completion of the post-acquisition data processing, a summary table including identified molecular ions, mass accuracy, retention time, peak intensity, and $^{TW}CCS_{N2,\ meas}$ was provided for each analyte by Unifi.

Validation of $^{TW}CCS_{N2,\ meas}$ values

A reference mix (SI, Table S4) was analyzed whenever a new data set was acquired to validate $^{TW}CSS_{N2,\ meas}$ values. If several sample sets were acquired in a single run, then three reference mix injections were distributed across the entire sequence to ensure no drift in $^{TW}CCS_{N2,\ meas}$ over time. If the mean $^{TW}CCS_{N2,\ meas}$ of each compound in the reference mix was within ± 2% from its previously determined and published value [28], then $^{TW}CCS_{N2,\ meas}$ determination of the entire sample set was considered acceptable. If not, then $^{TW}CCS_{N2}$ calibration and sample set(s) analysis were repeated.

Accuracy, precision, and mean absolute error of $^{TW}CCS_{N2,\ meas}$ versus $^{TW}CCS_{N2,\ pred}$

The accuracy (% bias) was calculated by dividing the difference between the mean $^{TW}CCS_{N2,\ meas}$ and $^{TW}CCS_{N2,\ pred}$ by the $^{TW}CCS_{N2,\ pred}$ which was further multiplied by a factor of 100. The precision of $^{TW}CCS_{N2,\ meas}$ was determined by the coefficient of variation (CV): the standard deviation (SD) between individual $^{TW}CCS_{N2}$ measurements divided by the mean $^{TW}CCS_{N2,\ meas}$ which was multiplied by a factor of 100. The mean absolute error was calculated by dividing the sum of absolute errors (difference between $^{TW}CCS_{N2,\ pred}$ and mean $^{TW}CCS_{N2,\ meas}$) by the number of investigated compounds. Error bars displayed in subsequent figures correspond to the obtained SD.

Results and discussion

In total, 165 compounds were incorporated into our assessment, and their CCS values ($^{TW}CCS_{N2}$) were determined following LC-IMS-MS analysis (SI, Table S5). The entire data set, covering an overall mass (*m/z*) and $^{TW}CCS_{N2}$ range of *m/z* 146–862 and 120–280 Å^2 respectively, was utilized to compare mean measured ($^{TW}CCS_{N2,\ meas}$) with predicted CCS ($^{TW}CCS_{N2,\ pred}$) values (see "Correlation between $^{TW}CCS_{N2,\ pred}$ and mean $^{TW}CCS_{N2,\ meas}$ values"). Moreover, a reduced data set ($n = 139$) was further used to verify if the previously observed repetitive shifts in relative $^{TW}CCS_{N2,\ meas}$ between parent drugs (or precursors) and their metabolites were biotransformation-specific. The selection and inclusion of those compounds for such assessment was conducted based on the possibility of creating compound pairs ($n = 86$; SI, Table S6) covering three common types of phase I biotransformation [hydroxylation ($n = 19$), N-oxidation ($n = 9$), demethylation ($n = 13$)] and five common phase II biotransformations [O-glucuronidation ($n = 14$), N-glucuronidation ($n = 9$), sulfation ($n = 10$), glutathione conjugation ($n = 7$), and acetylation ($n = 5$)]. Although most investigated compounds represented already marketed drugs and their corresponding metabolites, additional internal compounds were included for our assessment to extend the number of compound pairs for certain types of biotransformation. The only prerequisite for internal compound inclusion was to have synthesized reference material with a nuclear magnetic resonance-confirmed structure.

Reproducibility of $^{TW}CCS_{N2,\ meas}$ values

Similar to other published data [22, 29–31], the generated analyte-specific $^{TW}CCS_{N2,\ meas}$ values were highly reproducible over the entire period of our assessment (8 months) which was not only demonstrated with the reference mix used for system suitability testing (SI, Table S4 and Fig. S1) but also with the entire dataset (SI, Table S5). For the latter, the SD between individually determined $^{TW}CCS_{N2,\ meas}$ values (up to $n = 3$) was maximum 1.8 Å^2 resulting in a precision ≤ 1.0%.

Correlation between $^{TW}CCS_{N2,\ pred}$ and mean $^{TW}CCS_{N2,\ meas}$ values

After achieving excellent reproducibility in $^{TW}CCS_{N2,\ meas}$ values for our entire data set ($n = 165$), a better understanding of its accuracy was required. For this, mean $^{TW}CCS_{N2,\ meas}$ values were further compared with their $^{TW}CCS_{N2,\ pred}$ values (Waters CCSonDemand) which overall resulted in a good correlation ($R^2 = 0.9594$) as depicted in Fig. 1a. The obtained linear regression with a slope of 0.9036 (95% confidence intervals ranging from 0.8748 to 0.9323) and an intercept at + 18.14 (95% confidence intervals ranging from 12.49 to 23.78) was also close to its optimum (dashed black line). On the individual level, the obtained bias between $^{TW}CCS_{N2,\ pred}$ and mean $^{TW}CCS_{N2,\ meas}$ ranged from − 6.5 to + 11.9% (SI, Table S5) while the mean absolute error over the entire data set was 5.1%. The bias was within ± 10% (red area/dashed lines in Fig. 1) for 164 of the investigated compounds (99.4%). By further narrowing the acceptance criterion, most of the investigated compounds (87.3%, $n = 144$) met the ± 5% threshold (orange area/dotted lines in Fig. 1) while only 64.8% ($n = 107$) met the most stringent acceptance criterion of ± 3% (green area/solid lines in Fig. 1). It is worth mentioning that additional efforts were conducted to elucidate the origin of obtained bias in our presented data set. Neither the molecular weight (data not shown) nor an increase in $^{TW}CCS_{N2}$ could be identified as a root cause. The latter demonstrated an equal distribution in negative ($n = 93$) and positive bias ($n = 72$) over the investigated $^{TW}CCS_{N2}$ range (Fig. 1b). Hence, additional investigations would be necessary to clarify why certain $^{TW}CCS_{N2}$ values could not be predicted as accurately as other ones. Besides CCSonDemand, other computational tools or algorithms, previously reporting excellent correlations between CCS_{pred}

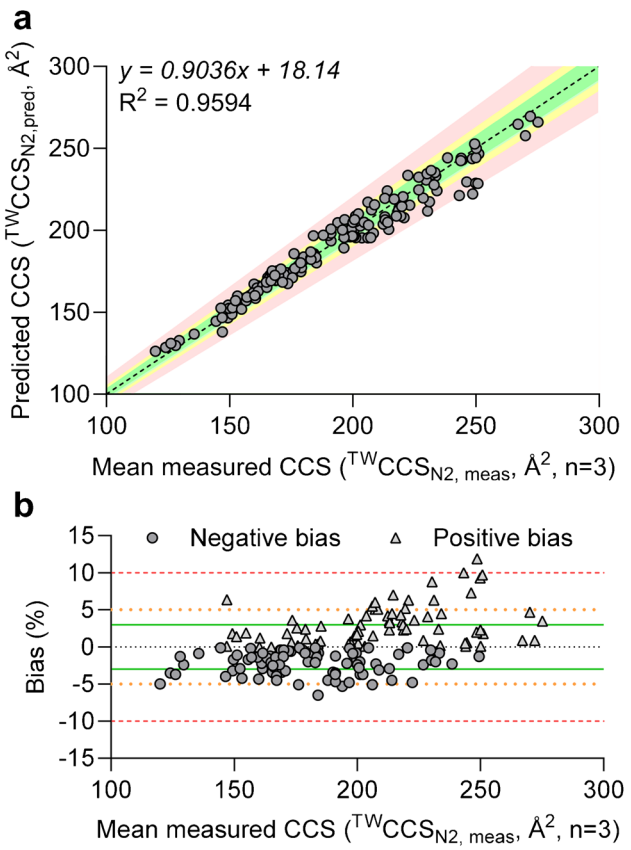

Fig. 1 **a** Correlation between predicted ($^{TW}CCS_{N2,\ pred}$) and mean measured CCS values ($^{TW}CCS_{N2,\ meas}$) for 165 investigated compounds. **b** Bias distribution across investigated $^{TW}CCS_{N2}$ range. The colored areas or lines represent the deviation of ± 10% (red/dashed), ± 5% (orange/dotted), and ± 3% (green/solid) from the optimum (dashed black line)

and CCS_{meas} values [32, 33], could further be tested with our publicly shared $^{TW}CCS_{N2,\ meas}$ values (SI, Table S5 or the separately provided.csv file in the online resources). Such assessment, however, was out of scope for this study. Overall, a high confidence was associated with the generated data set which was used for our assessment of biotransformation-specific relative shifts in $^{TW}CCS_{N2,\ meas}$ as discussed next.

Biotransformation-specific relative shifts in mean $^{TW}CCS_{N2,\ meas}$ values

An almost linear relationship between shifts in mean $^{TW}CCS_{N2,\ meas}$ values relative to the increase or decrease in mass was obtained for each type of investigated biotransformation (Fig. 2a). For instance, the elimination of a methyl group from the parent drug (− 14 Da) decreased the mean $^{TW}CCS_{N2,\ meas}$ relative to the parent drug or precursor by - 6.5 ± 2.1 Å^2 on average (Table 1). On the other hand, the mean $^{TW}CCS_{N2,\ meas}$ relative to the parent drug or precursor increased by + 13.5 ± 1.9 Å^2 on average following acetylation (+ 42 Da) while sulfation (+ 80 Da) increased the mean $^{TW}CCS_{N2,\ meas}$ in comparison to the parent drug or precursor even further (+ 17.9 ± 4.4 Å^2). Oxygenation as phase I biotransformation, including hydroxylation (+ 3.8 ± 1.4 Å^2) and N-oxidation (+ 3.4 ± 3.3 Å^2), also perfectly fitted into the almost linear relationship (Fig. 2a) which agreed with other published data [23]. However, both phase I biotransformations could not be differentiated from each other purely based on IMS-MS data since similar relative mean shifts in $^{TW}CCS_{N2,\ meas}$ were observed (Fig. 2b). Fortunately, other experiments such as hydrogen–deuterium exchange [34, 35] or selective reduction of N-oxides to amines with titanium (III) chloride [36] enable the discrimination between both types of biotransformation. Secondary ($n = 3$), tertiary ($n = 4$), and quaternary N-glucuronides ($n = 2$) included in our assessment exhibited on average a slightly higher relative mean shift in $^{TW}CCS_{N2,\ meas}$ (+ 41.7 ± 7.5 Å^2) compared to the investigated O-glucuronides (+ 38.1 ± 8.9 Å^2) with almost identical SDs (Table 1 and Fig. 2c). On some occasions, a much more discriminative relative shift in $^{TW}CCS_{N2,\ meas}$ values was obtained when the parent drug was either O- or N-glucuronidated (see "Potential to elucidate structural relationships between metabolites") while the tendency of N-glucuronides exhibiting higher relative shifts in $^{TW}CCS_{N2,\ meas}$ values compared to O-glucuronides remained constant.

It was further observed that the variation in relative mean shifts in $^{TW}CCS_{N2,\ meas}$ values was significantly increased for phase II compared to phase I biotransformations which was somehow expected: simple modifications following phase I reactions typically introduce relatively small changes in the molecular structure of the parent drug resulting in fairly consistent shifts in relative $^{TW}CCS_{N2,\ meas}$ values (except for major dealkylations within the molecule). On the other hand, conjugation of a large and rather flexible residue such as glutathione (tripeptide, + 305 Da) alters the molecular structure significantly which resulted in a mean relative $^{TW}CCS_{N2,\ meas}$ increase by + 49.2 ± 13.2 Å^2 on average (Table 1). Two main factors were identified as a potential origin of the increased variation in relative mean $^{TW}CCS_{N2,\ meas}$ shifts following phase II biotransformation: (i) bulky entities could exist in different gas phase conformations and (ii) the site of conjugation can further influence changes in relative mean $^{TW}CCS_{N2,\ meas}$ values. For instance, glucuronic acid conjugated to a flexible aliphatic side chain could have a significantly different $^{TW}CCS_{N2,\ meas}$ compared to its isobaric version where conjugation occurs on a rather rigid aromatic ring system (see example in "Potential to elucidate structural relationships between metabolites").

Nonetheless, almost non-overlapping bands in relative mean $^{TW}CCS_{N2,\ meas}$ shifts were obtained for each type of investigated biotransformation (Fig. 2a and Table 1). The

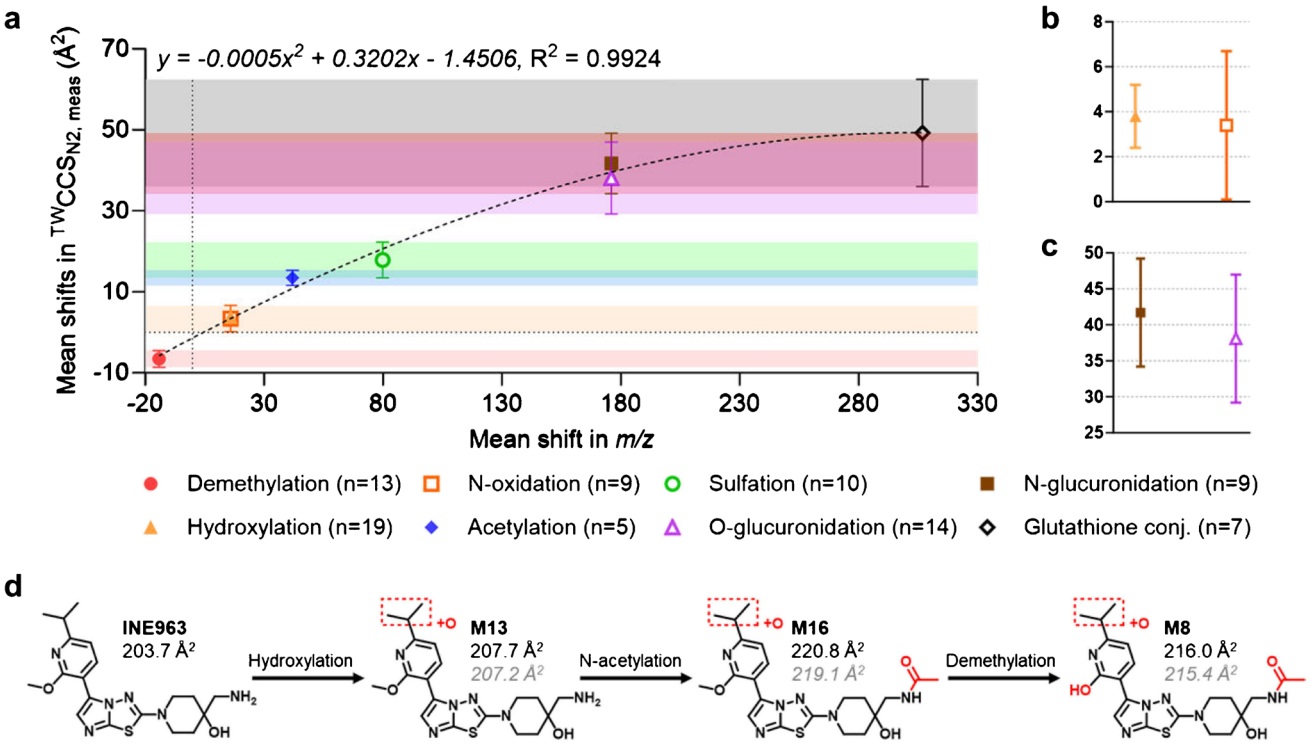

Fig. 2 **a** Correlation between mean measured mass changes and relative mean $^{TW}CCS_{N2,\ meas}$ shifts. Zoom into **b** hydroxylation and N-oxidation as well as **c** O- and N-glucuronidation. **d** Example for $^{TW}CCS_{N2}$ calculation (grey italics values) based on the obtained polynomial regression from **a** in comparison to $^{TW}CCS_{N2,\ meas}$ values (black values)

Table 1 Obtained mean *m/z* and relative mean $^{TW}CCS_{N2}$ shifts based on measured or predicted CCS values

Biotransformation	Mean measured shift in *m/z*	Relative mean shift in $^{TW}CCS_{N2}$ (Å^2) based on	
		$^{TW}CCS_{N2,\ meas}$	$^{TW}CCS_{N2,\ pred}$
Demethylation ($n=13$)	−14.0159 ± 0.0016	−6.5 ± 2.1	−4.8 ± 3.8
Hydroxylation ($n=19$)	+15.9946 ± 0.0013	+3.8 ± 1.4	+3.3 ± 3.1
N-oxidation ($n=9$)	+15.9948 ± 0.0007	+3.4 ± 3.3	+4.0 ± 2.2
Acetylation ($n=5$)	+42.0104 ± 0.0008	+13.5 ± 1.9	+9.9 ± 3.3
Sulfation ($n=10$)	+79.9602 ± 0.0113	+17.9 ± 4.4	+12.2 ± 4.5
O-glucuronidation ($n=14$)	+176.0313 ± 0.0036	+38.1 ± 8.9	+35.8 ± 5.8
N-glucuronidation ($n=9$)	+176.0299 ± 0.0061	+41.7 ± 7.5	+36.4 ± 7.0
Glutathione conjugation ($n=7$)	+306.7958 ± 0.7619	+49.2 ± 13.2	+52.6 ± 11.3

Corresponding raw data are provided as separate.csv file (see online resource "*Raw data for* Table 1")

plateau towards the upper end of the correlation between the mean measured mass and relative mean $^{TW}CCS_{N2,\ meas}$ shift was most likely caused by the underestimation of the $^{TW}CCS_{N2,\ meas}$ values for the glutathione conjugates which rather tend to be multiply charged instead of singly charged. It is noteworthy mentioning here that IMS and the CCS value of a molecule strongly depend on its charge state [29, 37]. For our work, however, the $^{TW}CCS_{N2,\ meas}$ of a singly charged ion from a metabolite had to be compared with the one of its parent drug (see also "Limitations"). The obtained relative mean $^{TW}CCS_{N2}$ shifts based on $^{TW}CCS_{N2,\ meas}$ values further agreed with the theoretical relative shifts when taking $^{TW}CCS_{N2,\ pred}$ values into consideration (Table 1 and SI, Fig. S2).

Based on the obtained polynomial regression ($y = -0.0005x^2 + 0.3202x - 1.4506$) between the mean measured mass changes and relative mean shifts in $^{TW}CCS_{N2,\ meas}$ (Fig. 2a), $^{TW}CCS_{N2}$ values of metabolites could readily be calculated which is illustrated for an internal compound in Fig. 2d: the $^{TW}CCS_{N2}$ of the parent drug (INE963) following hydroxylation was calculated 207.2 Å^2

($^{TW}CCS_{N2, calc}$) which agreed with the actual $^{TW}CCS_{N2, meas}$ for metabolite M13 (207.7 Å^2). Even after subsequent N-acetylation and demethylation of M13, resulting in metabolite M8, the $^{TW}CCS_{N2, calc}$ (215.4 Å^2) was in excellent agreement with the $^{TW}CCS_{N2, meas}$ (216.0 Å^2). Hence, the discovered biotransformation-specific relative shifts in mean $^{TW}CCS_{N2, meas}$ values (and the combination thereof) can also be considered for metabolite assignment/confirmation (rather than their absolute $^{TW}CCS_{N2, meas}$ values) complementing the conventional approach where changes in *m/z* values are compared. Only for glucuronidation or glutathione conjugation, special care must be taken exhibiting increased variabilities and slightly overlapping bands in relative mean $^{TW}CCS_{N2, meas}$ shifts (Fig. 2a and Table 1).

Similar biotransformation-specific shifts in relative $^{TW}CCS_{N2, meas}$ obtained on fragment ion level

Identical biotransformation-specific shifts in relative $^{TW}CCS_{N2, meas}$ were also obtained on fragment ion level as illustrated for hydroxylation, demethylation, and N-acetylation in Fig. 3. Phase II biotransformations such as sulfation and glucuronidation were not considered for this assessment since the major fragment ion from such metabolites is often only the parent drug or corresponding precursor following the characteristic neutral loss of the sulfate (80 Da, SO_3) or the glycone (176 Da, $C_6H_8O_6$), respectively [38–41]. One prerequisite for the assessment of biotransformation-specific shifts in relative $^{TW}CCS_{N2, meas}$ on fragment ion level was the presence of common fragment ions between the metabolite and parent drug or precursor (with and without the biotransformation). The relative shift in $^{TW}CCS_{N2, meas}$ for mephenytoin after hydroxylation, leading to 4-hydroxy mephenytoin, was + 4.1 Å^2 on precursor ion level (Fig. 3a). An almost identical relative shift (+ 3.4 Å^2) was obtained after comparing the $^{TW}CCS_{N2, meas}$ values of the major fragment ion for mephenytoin at *m/z* 134 and 4-hydroxy mephenytoin at *m/z* 150 (Fig. 3b). For demethylation, the relative shifts in $^{TW}CCS_{N2, meas}$ between diazepam and nordazepam on precursor and fragment ion level were again in the similar range: − 4.6 Å^2 on precursor ion level (Fig. 3c) and − 3.8 Å^2 on fragment ion level (Fig. 3d) considering the fragment ions at *m/z* 222 and *m/z* 208 for diazepam and nordazepam, respectively. The best agreement in biotransformation-specific relative shifts in $^{TW}CCS_{N2, meas}$ determined on precursor (+ 8.1 Å^2, Fig. 3e) and fragment ion level (+ 8.0 Å^2, Fig. 3f) was obtained with an internal compound (NVS1) and its N-acetylated metabolite M7. The combination of fragment ion $^{TW}CCS_{N2, meas}$ values, allowing the discrimination of ortho-, para-, or meta-conjugated metabolites due to minor changes in $^{TW}CCS_{N2, meas}$ values [16] and the potential to utilize relative shifts in $^{TW}CCS_{N2,meas}$ values for metabolite mapping purposes (see "Potential to elucidate structural relationships between metabolites"), would represent a powerful analytical tool for future metabolism studies to elucidate structural relationships between positional isomers and their subsequently conjugated metabolites, e.g., glucuronides.

Potential to elucidate structural relationships between metabolites

One major benefit to considering relative shifts in $^{TW}CCS_{N2, meas}$ values for biotransformation studies is the potential to elucidate structural relationships between metabolites in order to design metabolic pathways. During

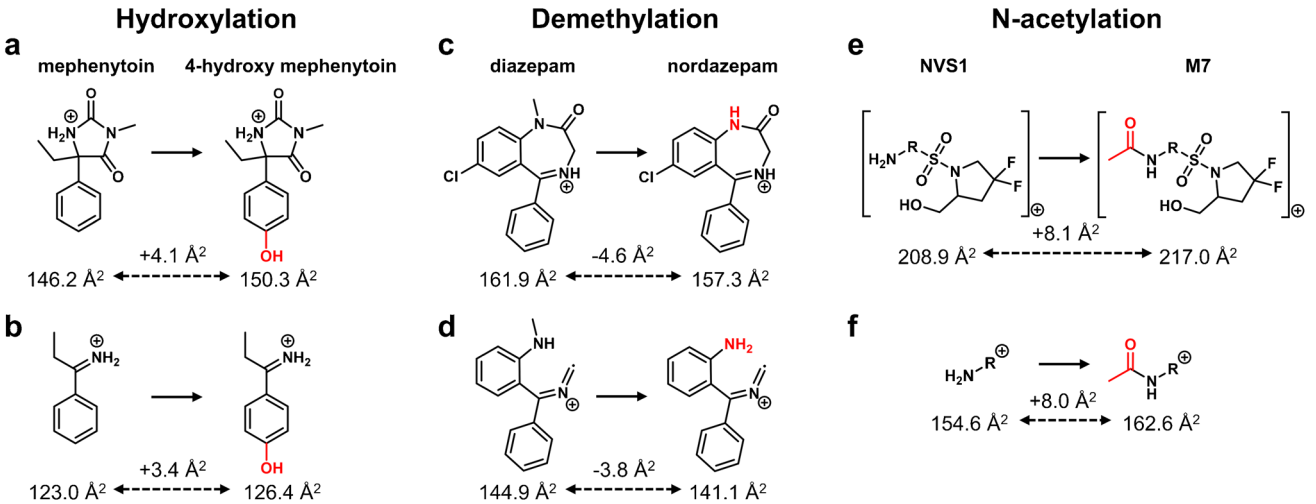

Fig. 3 Biotransformation-specific shifts in relative $^{TW}CCS_{N2, meas}$ values obtained either on precursor ion (**a**, **c**, **e**) or fragment ion level (**b**, **d**, **f**) exemplified for hydroxylation, demethylation, and N-acetylation (proposals for charge localization and fragment ion structures are only tentative)

in vivo metabolism assessment of an internal compound (NVS1), several hydroxylated and glucuronidated metabolites were detected in pooled plasma samples (AUC0-24 h) following oral (rat) and intravenous administration (dog), respectively. In both studies, conventional MS fragmentation did not assist in structure elucidation and made the localization of the biotransformation impossible since similar product ion spectra were obtained (data not shown). In contrast, relative shifts in $^{TW}CCS_{N2,\ meas}$ values provided hints about their structural relationships (Fig. 4). The direct O-glucuronide (M2) was conjugated to a rather flexible side chain whereas the N-glucuronide (M4) was conjugated to a rigid aromatic ring system. Consequently, both direct glucuronides exhibited different $^{TW}CCS_{N2,\ meas}$ values (234.3 Å^2 for M2 and 254.1 Å^2 for M4). By knowing that hydroxylation of NVS1, leading to metabolite M1, increased the $^{TW}CCS_{N2,\ meas}$ by + 6.2 Å^2 relative to the parent drug, structural relationships of the detected hydroxylated and glucuronidated metabolites (M9, M10 and M11) relative to both direct glucuronides could readily be elucidated: the differences in $^{TW}CCS_{N2,\ meas}$ of M10 (+25.2 Å^2) and M11 (+25.4 Å^2) were too high to originate from M2 (O-glucuronide). On the other hand, when the $^{TW}CCS_{N2,\ meas}$ of M10 (259.5 Å^2) and M11 (259.7 Å^2) were compared to the N-glucuronide (M4), then the relative shifts in $^{TW}CCS_{N2,\ meas}$ values matched with the expected one for NVS1 hydroxylation (+5.4 Å^2 for M10 and +5.6 Å^2 for M11). Consequently, M10 and M11 were most likely structurally related to M4. On the other hand, M9 was most likely structurally related to M2.

Limitations

Despite the above-highlighted benefits to consider relative shifts in $^{TW}CCS_{N2,\ meas}$ values for biotransformation assignment/confirmation and metabolite mapping purposes, several limitations are also associated with the presented methodology: (i) biotransformation-specific relative shifts in $^{TW}CCS_{N2,\ meas}$ values could only be obtained when $^{TW}CCS_{N2,\ meas}$ values of the same ion species were compared with each other. It is not recommended to compare the $^{TW}CCS_{N2,\ meas}$ of a protonated parent drug with one of its deprotonated metabolites. Moreover, $^{TW}CCS_{N2,\ meas}$ comparison of a protonated parent drug with the sodium or potassium adduct of its metabolite will neither be successful. (ii) So far only singly charged ions were considered for our assessment. Nevertheless, this already allowed the comparison of a broad range of parent drugs/precursors with their corresponding metabolites since low molecular-weighted drugs with a mass of up to 500–600 Da tend to be mainly singly charged. For future activities, the proposed concept of biotransformation-specific relative shifts in $^{TW}CCS_{N2,\ meas}$ values may also need to be verified for multiple charged ions. (iii) The current data set is still rather limited and needs to be further extended, e.g., by either adding more compound pairs to already investigated types of biotransformation or by incorporating additional types of biotransformation such as dealkylation reaction causing a significantly greater loss in mass.

Conclusions

The emerging role of highly reproducible CCS values, as an instrument and analytical method-independent physicochemical property of a molecule, becomes much more evident in various research domains. In our opinion, this should also be considered more frequently for biotransformation studies. Such analyte-specific parameters enable metabolite alignment between various biotransformation studies conducted at diverse analytical labs at different drug development stages. By accessing publicly available computational tools such as Waters CCSonDemand, accurate $^{TW}CCS_{N2}$ value prediction also seems nowadays possible eliminating the need to determine them experimentally.

More importantly, however, is to consider relative shifts in $^{TW}CCS_{N2,\ meas}$ between a parent drug (or any precursor) and its corresponding metabolite rather than their absolute $^{TW}CCS_{N2,\ meas}$ values: constant and discriminative relative mean shifts in $^{TW}CCS_{N2,\ meas}$ values apparently exist as demonstrated for eight different phase

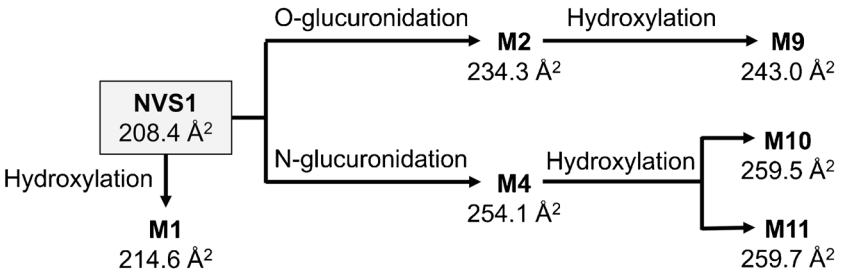

Fig. 4 Potential of relative shifts in $^{TW}CCS_{N2,\ meas}$ values to elucidate structural relationships between metabolites as illustrated with an internal compound (NVS1) and its in vivo obtained hydroxylated and glucuronidated metabolites. Please note that the displayed mapping is based on relative changes in $^{TW}CCS_{N2,\ meas}$ and not on enzymatic formation (hydroxylation with subsequent glucuronidation)

I and II biotransformation which were not only obtained on precursor ion but also on fragment ion level. In the perspective of metabolism studies, such biotransformation-specific relative shifts in $^{TW}CCS_{N2,\ meas}$ would mainly have two major benefits: (i) allowing metabolite identification/confirmation as an orthogonal approach to the conventional comparison of changes in *m/z* values. (ii) The mapping of metabolites in metabolic pathways can significantly be simplified. This would especially be important whenever isobaric metabolites are present, sharing multiple and similar combinations of phase I and II biotransformation but on different molecule locations, which unfortunately cannot be distinguished from each other due to identical MS fragmentation patterns. A simpler metabolite mapping process would be of particular importance for low-abundant circulating metabolites where no synthetic reference material is readily available due to either challenging biosynthesis or resource restrictions. Moreover, in perspective of regulatory guidelines from health authorities, e.g., EMA DDI guidance, demanding to elucidate 90% of detected metabolites in human excreta, the comparison of relative shifts in $^{TW}CCS_{N2,\ meas}$ to map metabolites correctly would further reduce additional experiments to fully characterize relevant metabolites.

Supplementary Information The online version contains supplementary material available at https://doi.org/10.1007/s00216-023-05063-1.

Acknowledgements The authors would like to express their deep gratitude to Tobias Kaster, Julien Bourgailh, Gaelle Chenal, and Judith Streckfuss (PK Sciences, Novartis, Basel) for sharing reference material of commercially available and internal compounds. Moreover, we would like to acknowledge Russell Mortishire-Smith, David Higton, Mario Mergelsberg, Julien Bourquin, and Arun K from Waters for their constant support.

Author contribution All authors contributed to the study conception and design. Material preparation, data collection, and analysis were performed by Raphael Schütz, Christian Lanshoeft, and Frédéric Lozac'h. The first draft of the manuscript was written by Christian Lanshoeft and all authors commented on previous versions of the manuscript. All authors read and approved the final manuscript.

Funding The work was funded by Novartis Pharma AG (Basel, Switzerland).

Data availability All data generated and analyzed during this work are included in this published article and its supplementary information files.

Declarations

Ethics approval Both preclinical studies of NVS1 were conducted in compliance with the Animal Welfare Act, the Guide for the Care and Use of Laboratory Animals, and the Office of Laboratory Animal Welfare and in accordance with the Novartis Animal Care and Use Committee (NACUC).

Competing interests The authors declare no competing interests.

References

1. U.S. Food and Drug Administration (FDA). Clinical pharmacology: considerations for human radiolabeled mass balance studies - guidance for industry. 2022.
2. U.S. Food and Drug Administration (FDA). Safety testing of drug metabolites - guidance for industry revision 2. 2020.
3. European Medicines Agency (EMA). Guideline on the investigation of drug interactions. 2012.
4. International Conference on Harmonization (ICH). M3(R2) Non-clinical safety studies for the conduct of human clinical trials and marketing authorization for pharmaceuticals. 2013.
5. Luffer-Atlas D, Atrakchi A. A decade of drug metabolite safety testing: industry and regulatory shared learning. Expert Opin Drug Metab Toxicol. 2017;13(9):897–900. https://doi.org/10.1080/17425255.2017.1364362.
6. Ma S, Chowdhury SK. A tiered approach to address regulatory drug metabolite-related issues in drug development. Bioanalysis. 2014;6(5):587–90. https://doi.org/10.4155/bio.14.40.
7. Schadt S, Bister B, Chowdhury SK, Funk C, Hop CECA, Humphreys WG, et al. A decade in the MIST: learnings from investigations of drug metabolites in drug development under the "metabolites in safety testing" regulatory guidance. Drug Metab Dispos. 2018;46(6):865–78. https://doi.org/10.1124/dmd.117.079848.
8. Pearson D, Weiss HM, Jin Y, van Lier JJ, Erpenbeck VJ, Glaenzel U, et al. Absorption, distribution, metabolism, and excretion of the oral prostaglandin D2 receptor 2 antagonist fevipiprant (QAW039) in healthy volunteers and in vitro. Drug Metab Dispos. 2017;45(7):817–25. https://doi.org/10.1124/dmd.117.075358.
9. James AD, Schiller H, Marvalin C, Jin Y, Borell H, Roffel AF, et al. An integrated assessment of the ADME properties of the CDK4/6 inhibitor ribociclib utilizing preclinical in vitro, in vivo, and human ADME data. Pharmacol Res Perspect. 2020;8(3):e00599. https://doi.org/10.1002/prp2.599.
10. Zhang JY, Zhang J, Kiffe M, Walles M, Jin Y, Blanz J, et al. Preclinical pharmacokinetics and metabolism of MAK683, a clinical stage selective oral embryonic ectoderm development (EED) inhibitor for cancer treatment. Xenobiotica. 2022;52(1):65–78. https://doi.org/10.1080/00498254.2021.2005852.
11. D'Atri V, Causon T, Hernandez-Alba O, Mutabazi A, Veuthey J-L, Cianferani S, et al. Adding a new separation dimension to MS and LC–MS: what is the utility of ion mobility spectrometry? J Sep Sci. 2018;41(1):20–67. https://doi.org/10.1002/jssc.201700919.
12. Ross DH, Xu L. Determination of drugs and drug metabolites by ion mobility-mass spectrometry: a review. Anal Chim Acta. 2021;1154:338270. https://doi.org/10.1016/j.aca.2021.338270.
13 Cumeras R, Figueras E, Davis CE, Baumbach JI, Gràcia I. Review on ion mobility spectrometry. Part 1: current instrumentation. Analyst. 2015;140(5):1376–90. https://doi.org/10.1039/c4an01100g.

14. Blech S, Laux R. Resolving the microcosmos of complex samples: UPLC/travelling wave ion mobility separation high resolution mass spectrometry for the analysis of in vivo drug metabolism studies. Int J Ion Mobil Spectrom. 2013;16:5–17. https://doi.org/10.1007/s12127-012-0113-1.
15. Hadavi D, Borzova M, Porta Siegel T, Honing M. Uncovering the behaviour of ions in the gas-phase to predict the ion mobility separation of isomeric steroid compounds. Anal Chim Acta. 2022;1200:339617. https://doi.org/10.1016/j.aca.2022.339617.
16. Cuyckens F, Wassvik C, Mortishire-Smith RJ, Tresadern G, Campuzano I, Claereboudt J. Product ion mobility as a promising tool for assignment of positional isomers of drug metabolites. Rapid Commun Mass Spectrom. 2011;25(23):3497–503. https://doi.org/10.1002/rcm.5258.
17. de Bruin CR, Hennebelle M, Vincken J-P, de Bruijn WJC. Separation of flavonoid isomers by cyclic ion mobility mass spectrometry. Anal Chim Acta. 2023;1244:340774. https://doi.org/10.1016/j.aca.2022.340774.
18. Higton D, Palmer ME, Vissers JPC, Mullin LG, Plumb RS, Wilson ID. Use of cyclic ion mobility spectrometry (cIM)-mass spectrometry to study the intramolecular transacylation of diclofenac acyl glucuronide. Anal Chem. 2021;93(20):7413–21. https://doi.org/10.1021/acs.analchem.0c04487.
19. Kováč A, Majerová P, Nytka M, Cechová MZ, Bednář P, Hájek R, et al. Separation of isomeric tau phosphopeptides from Alzheimer's disease brain by cyclic ion mobility mass spectrometry. J Am Soc Mass Spectrom. 2023;34(3):394–400. https://doi.org/10.1021/jasms.2c00289.
20. Giles K, Ujma J, Wildgoose J, Pringle S, Richardson K, Langridge D, et al. A cyclic ion mobility-mass spectrometry system. Anal Chem. 2019;91(13):8564–73. https://doi.org/10.1021/acs.analchem.9b01838.
21. Stojko J, Fieulaine S, Petiot-Bécard S, Van Dorsselaer A, Meinnel T, Giglione C, et al. Ion mobility coupled to native mass spectrometry as a relevant tool to investigate extremely small ligand-induced conformational changes. Analyst. 2015;140(21):7234–45. https://doi.org/10.1039/c5an01311a.
22. Paglia G, Williams JP, Menikarachchi L, Thompson JW, Tyldesley-Worster R, Halldórsson S, et al. Ion mobility derived collision cross sections to support metabolomics applications. Anal Chem. 2014;86(8):3985–93. https://doi.org/10.1021/ac500405x.
23. Ross DH, Seguin RP, Xu L. Characterization of the impact of drug metabolism on the gas-phase structures of drugs using ion mobility-mass spectrometry. Anal Chem. 2019;91(22):14498–507. https://doi.org/10.1021/acs.analchem.9b03292.
24. Hamilton RA, Garnett WR, Kline BJ. Determination of mean valproic acid serum level by assay of a single pooled sample. Clin Pharmacol Ther. 1981;29(3):408–13. https://doi.org/10.1038/clpt.1981.56.
25. Bush MF, Campuzano IDG, Robinson CV. Ion mobility mass spectrometry of peptide ions: effects of drift gas and calibration strategies. Anal Chem. 2012;84(16):7124–30. https://doi.org/10.1021/ac3014498.
26. Connolly JRFB, Munoz-Muriedas J, Lapthorn C, Higton D, Vissers JPC, Webb A, et al. Investigation into small molecule isomeric glucuronide metabolite differentiation using in silico and experimental collision cross-section values. J Am Soc Mass Spectrom. 2021;32(8):1976–86. https://doi.org/10.1021/jasms.0c00427.
27. Broeckling CD, Yao L, Isaac G, Gioioso M, Ianchis V, Vissers JPC. Application of predicted collisional cross section to metabolome databases to probabilistically describe the current and future ion mobility mass spectrometry. J Am Soc Mass Spectrom. 2021;32(3):661–9. https://doi.org/10.1021/jasms.0c00375.
28. Higton D, Lanshoeft C, Lozac'h F. Use of predicted versus measured CCS values from different instrument platforms, and isomer separation on the Select Series Cyclic IMS. Waters Application Note 720007514. 2022.
29. Stow SM, Causon TJ, Zheng X, Kurulugama RT, Mairinger T, May JC, et al. An interlaboratory evaluation of drift tube ion mobility–mass spectrometry collision cross section measurements. Anal Chem. 2017;89(17):9048–55. https://doi.org/10.1021/acs.analchem.7b01729.
30. Morris CB, May JC, Leaptrot KL, McLean JA. Evaluating separation selectivity and collision cross section measurement reproducibility in helium, nitrogen, argon, and carbon dioxide drift gases for drift tube ion mobility–mass spectrometry. J Am Soc Mass Spectrom. 2019;30(6):1059–68. https://doi.org/10.1007/s13361-019-02151-4.
31. Fiebig L, Laux R. A collision cross section and exact ion mass database of the formulation constituents polyethylene glycol 400 and polysorbate 80. Int J Ion Mobil Spectrom. 2016;19:131–7. https://doi.org/10.1007/s12127-016-0195-2.
32. Song X-C, Dreolin N, Canellas E, Goshawk J, Nerin C. Prediction of collision cross-section values for extractables and leachables from plastic products. Environ Sci Technol. 2022;56(13):9463–73. https://doi.org/10.1021/acs.est.2c02853.
33. Ross DH, Seguin RP, Krinsky AM, Xu L. High-throughput measurement and machine learning-based prediction of collision cross sections for drugs and drug metabolites. J Am Soc Mass Spectrom. 2022;33(6):1061–72. https://doi.org/10.1021/jasms.2c00111.
34. Ohashi N, Furuuchi S, Yoshikawa M. Usefulness of the hydrogen–deuterium exchange method in the study of drug metabolism using liquid chromatography-tandem mass spectrometry. J Pharm Biomed Anal. 1998;18(3):325–34. https://doi.org/10.1016/S0731-7085(98)00092-2.
35. Sonawane D, Reddy A, Jadav T, Sahu AK, Tekade RK, Sengupta P. Advancements in practical and scientific bioanalytical approaches to metabolism studies in drug development. Bioanalysis. 2021;13(11):913–30. https://doi.org/10.4155/bio-2021-0050.
36. Kulanthaivel P, Barbuch RJ, Davidson RS, Yi P, Rener GA, Mattiuz EL, et al. Selective reduction of N-oxides to amines: application to drug metabolism. Drug Metab Dispos. 2004;32(9):966–72.
37. Siems WF, Viehland LA, Hill HH. Correcting the fundamental ion mobility equation for field effects. Analyst. 2016;141(23):6396–407. https://doi.org/10.1039/c6an01353h.
38. Fitzgerald CCJ, Hedman R, Uduwela DR, Paszerbovics B, Carroll AJ, Neeman T, et al. Profiling urinary sulfate metabolites with mass spectrometry. Front Mol Biosci. 2022;9:829511. https://doi.org/10.3389/fmolb.2022.829511.
39. Wen H, Yang H, An YJ, Kim JM, Lee DH, Jin X, et al. Enhanced phase II detoxification contributes to beneficial effects of dietary restriction as revealed by multi-platform metabolomics studies. Mol Cell Proteomics. 2013;12(3):575–86. https://doi.org/10.1074/mcp.M112.021352.
40. Correia MSP, Lin W, Aria AJ, Jain A, Globisch D. Rapid preparation of a large sulfated metabolite library for structure validation in human samples. Metabolites. 2020;10(10):415. https://doi.org/10.3390/metabo10100415.
41. Feng X, Li Y, Guang C, Qiao M, Wang T, Chai L, et al. Characterization of the in vivo and in vitro metabolites of linarin in rat biosamples and intestinal flora using ultra-high performance liquid chromatography coupled with quadrupole time-of-flight tandem mass spectrometry. Molecules. 2018;23(9):2140. https://doi.org/10.3390/molecules23092140.